energies

MDPI

Article

Short-Circuit Fault Analysis of the Sen Transformer Using Phase Coordinate Model

Liang Bu, Song Han * and Jinling Feng

Department of Electrical Engineering, Guizhou University, Guiyang 550025, China; fengde556@gmail.com (L.B.); fengjl_1997@163.com (J.F.)
* Correspondence: shan@gzu.edu.cn

Abstract: The Sen Transformer (ST) provides an economical solution for power flow control and voltage regulation. However, fault analysis and evaluation of the performance of the transmission protection system in the presence of a ST have not been investigated. Hence, a short-circuit model of the ST using the phase coordinate method is proposed in this paper. Firstly, according to the coupled-circuit ST model, the nodal admittance matrix between the sending end and receiving end of the ST was deduced. Subsequently, a fully decoupled mathematical model was established that can reflect three characteristics, including its winding connection structure, electrical parameters, and ground impedance. Thus, with the help of the phase-coordinate-based solving methodology, a short-circuit ST model may be built for various short-circuit faults. The MATLAB and PSCAD/EMTDC software were employed to carry out simulated analyses for an equivalent two-bus system. The short-circuit currents obtained from the time-domain simulation and the analytic calculation utilizing the proposed model reached an acceptable agreement, confirming the simulation's effectiveness. Moreover, the variation of the fault currents with the variation of the compensating voltage after single-phase-to-ground and three-phase short-circuit faults was demonstrated and used to analyze the effect of the ST on the fault currents.

Keywords: decoupled mathematical model; nodal admittance matrix; phase coordinate method; Sen Transformer; short-circuit fault analysis

Citation: Bu, L.; Han, S.; Feng, J. Short-Circuit Fault Analysis of the Sen Transformer Using Phase Coordinate Model. *Energies* **2021**, *14*, 5638. https://doi.org/10.3390/en14185638

Academic Editor: Gianfranco Chicco

Received: 7 August 2021
Accepted: 4 September 2021
Published: 8 September 2021

1. Introduction

With the rapidly growing penetration of renewable energy sources and the ever-increasing complexity of electrical systems, transmission lines are becoming overloaded and experiencing reduced stability, increased voltage variation, and loop-flow of power. This fact is even more pronounced in large-scale power systems [1–4]. The demands for better utilization of existing power systems and to increase power transfer capability by installing flexible AC transmission system (FACTS) devices have become increasingly urgent. The Sen Transformer (ST), which can provide an independent and bidirectional active and reactive power flow control in a transmission line, has been proven to be reliable and cost-effective when compared with the emerging technology of VSC [5–7]. However, the complicated operational modes of the ST and the unique winding connections create some challenges for the fault analysis of power systems with STs. Therefore, it is necessary to establish a short-circuit model for the ST to properly evaluate its influence on fault currents.

From the perspective of the modeling of the ST and its variants, a power flow model of a ST was developed to study the impact of the ST for congestion management and ATC enhancement [8,9]. A steady-state model of a power-transistor-assisted ST(TAST) was established in [10,11], and power flow control for congestion management using TAST was performed in [12]. In addition, a power flow model of the extended ST(EST) was proposed in [13] for power flow analysis in a large-scale power system. However, these models are only suitable for steady-state analysis of power systems involving STs,

and fault analysis cannot be performed with the help of these models. For the transient analysis of the ST, a ST digital simulation model was developed using the PSCAD/EMTDC software package [14] and a new algorithm capable of selecting the best combination of tap settings was implemented in it. A detailed electromagnetic transient model was developed in [15] for the ST embedded in a network, but the detailed flux paths in the core were not considered in these models. Furthermore, an electromagnetic transient model for the ST based on the real-time high-fidelity magnetic equivalent circuit was proposed in [16] and estimated on the field-programmable gate array (FPGA) for hardware-in-the-loop applications. Meanwhile, in order to explore the internal characteristics of the ST, an analytical electromagnetic model considering the multi-winding coupling in the ST with a three-phase, three-limb structure was presented in [17]. Additionally, the application of high-power electronic on-load tap-changers in ST was introduced in [18] and a switching transient model was proposed for studying the commutation process. In [19], a quasi-steady-state model of a three-phase five-limb ST (TPFLST) is proposed, applying the principle of duality to evaluate the performance of a TPFLST with unbalanced load conditions. Nevertheless, there has been not much study on the fault analysis of a power system with a ST reported in the published literature. Although the electromagnetic transient ST models proposed in the existing literature can be used for short-circuit analysis, the electromagnetic transient calculations are tedious and time-consuming, especially in large-scale and complex power systems. There is an urgent need to develop a suitable method for short-circuit analysis of power systems containing STs.

From the perspective of short-circuit fault analysis methods, the symmetrical component-based method has been widely applied to perform fault analysis for multiphase distribution networks [20,21]. Moreover, regarding electrical equipment such as the transformer, superconducting fault current limiter, and permanent-magnet synchronous machine, the relevant fault models for carrying out short-circuit studies via symmetrical components are also presented in [22–24]. Although symmetrical components afford an admirable degree of unbalanced design and system operation, the assembly of sequence networks and the solution of sequence equations are not always easy, particularly in the case of a system as distinct from load unbalance when mutual coupling exists between the sequence networks [25–27]. Meanwhile, as for the three-phase, three-limb model of the ST, it should be noted that the magnetic coupling among all windings of the ST results in its unbalanced three-phase operation [17]. The method of symmetrical sequences may not be as accurate as expected in this case. The phase coordinate method was considered to be an attractive methodology to solve this problem, having been previously employed to model the conventional transformer, three-phase autotransformer, and synchronous machine [28–31] for short-circuit fault analysis. Hence, it may be an effective way to accurately calculate the short-circuit currents when a ST is installed in a power system, with the aid of the phase coordinate method.

Therefore, this paper proposes a short-circuit model of the ST, utilizing the phase coordinate method according to the different fault types. The contributions of this paper are:

1. A fully decoupled mathematical model of the ST is deduced based on the coupled circuit, considering the mutual inductances among all windings for the ST and the ground impedance on the secondary side of the ST.
2. Short-circuit models involving single ST faults and combined ST faults are proposed.
3. Variations of short-circuit current after the occurrence of single-phase-to-ground and three-phase-to-ground faults in a power system with a ST are presented, and the reasons for these variations are analyzed.

This paper is organized as follows. Section 2 presents a fully decoupled mathematical model of a ST for the phase coordinate method, and the ground impedance on the primary side of the ST is extended in this model. The short-circuit calculation for an electric power network using the phase coordinate method is described in Section 3. In Section 4, case studies are implemented to illustrate the effectiveness of the proposed short-circuit ST

model and analyze the variations of short-circuit current magnitude for single-phase-to-ground and three-phase short-circuit faults caused by the ST. Finally, the conclusions of this work are drawn in Section 5.

2. A Fully Decoupled Mathematical Model of ST for Phase Coordinate Method

2.1. The Working Principle of the ST

The basic topology structure of the ST is shown in Figure 1a. The voltages U_{sA}, U_{sB}, and U_{sC} at any point in the transmission lines supply to the Y-connected primary windings of the ST in phases A, B, and C, respectively. These primary windings constitute the exciting unit. A total of nine secondary windings with tap changers constitute the compensating voltage unit. Each limb of the core has three of the secondary windings, i.e., a1, a2, and a3 are placed on the limb of phase A; b1, b2, and b3 are placed on the limb of phase B; and c1, c2, and c3 are placed on the limb of phase C. The vector diagram for the ST's operation is shown in Figure 1b. As for phase A, the series-connected compensating voltage is as follows: $U_{ss'A} = U_{a1} + U_{b1} + U_{c1}$. Since there is a 120° phase shift between the induced voltages U_{a1}, U_{b1}, and U_{c1}, the sum of three voltage vectors can be varied by adjusting the tap changers in the secondary windings. Consequently, the obtained $U_{ss'A}$ becomes variable in magnitude and in the phase angle from 0° to 360°. In this way, the series-connected compensating voltages $U_{ss'B}$ and $U_{ss'C}$ in phases B and C can also be derived. Furthermore, the four-quadrant adjustment of the sending end voltage from U_s to $U_{s'}$ can be realized, i.e., $U_{s'} = U_s + U_{ss'}$.

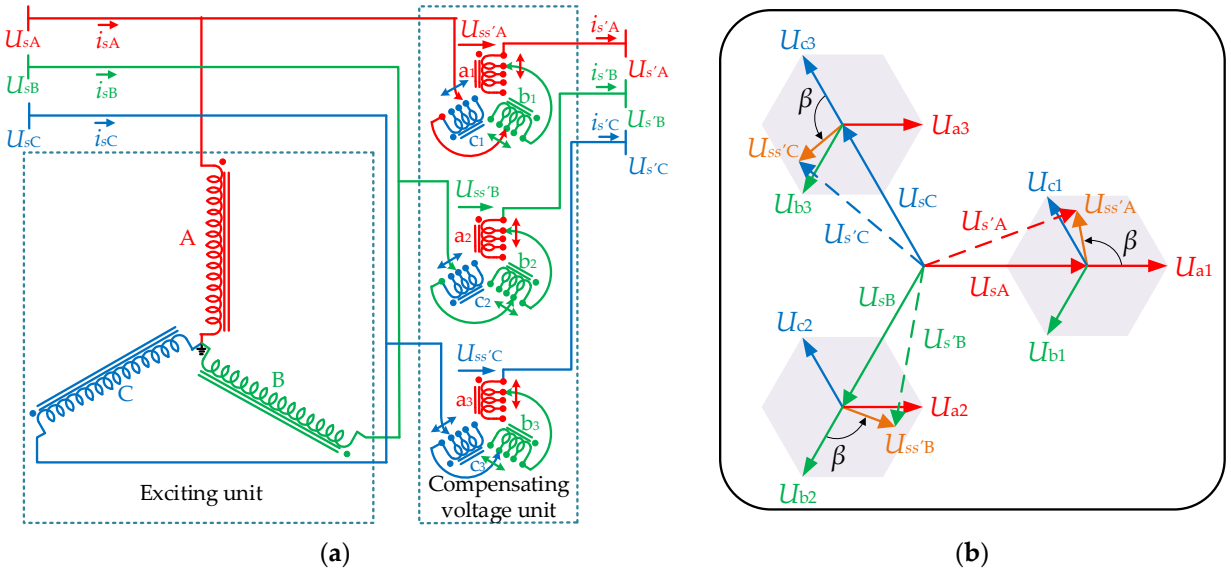

Figure 1. (**a**) The basic topology structure of the ST; (**b**) the vector diagram for the ST's operation.

By varying the magnitude of $U_{ss'}$ and the phase angle, β, of the injected compensating voltage, the three operational modes for the ST can be achieved: voltage regulation, phase angle regulation, and independent power-flow regulation [6,7].

- Voltage regulation mode. If the ST works as a voltage regulator, the phase voltage U_s is added to $U_{s'}$ by injecting the compensating voltage $U_{ss'}$, and $U_{ss'}$ is either in phase ($\beta = 0°$) or out of phase ($\beta = 180°$) with U_s.
- Phase angle regulation mode. When the ST is operating in the phase angle regulation mode, the series-connected compensating voltage $U_{ss'}$ is added to the transmission line in quadrature with U_s ($\beta = \pm 90°$).
- Independent power-flow regulation mode. If the ST is used as a power flow regulator, the active and the reactive power flows are regulated independently by changing U_s

to $U_{s'}$ by varying the magnitude and phase angle of the injected voltage $U_{ss'}$. The required $U_{ss'}$ can be derived from the desired active and reactive power.

2.2. Modeling of ST for Phase Coordinate Method

The coupled circuit of the ST is displayed in Figure 2. L_a, L_b, and L_c denote the self-inductances for the primary windings in phases A, B, and C, respectively. L_{a1}, L_{a2}, L_{a3}; L_{b1}, L_{b2}, L_{b3}; and L_{c1}, L_{c2}, and L_{c3} denote the self-inductances for the ST secondary windings in phases A, B, and C, respectively. M_{ij} represents the mutual inductance between windings i and j, where i, j = A, B, C, a1, a2, a3, b1, b2, b3, c1, c2, and c3, and it should be noted that i≠j. U_{pA}, U_{pB}, and U_{pC} represent the exciting voltages for the ST in phases A, B, and C, respectively. $U_{ss'A}$, $U_{ss'B}$, and $U_{ss'C}$ stand for the series-connected compensating voltages for the transmission line in phases A, B, and C, respectively. i_{pA}, i_{pB}, and i_{pC} represent the exciting currents for the ST in phases A, B, and C, respectively. $i_{s'A}$, $i_{s'B}$, and $i_{s'C}$ stand for the currents of the transmission line at the receiving end of the ST in phases A, B, and C, respectively.

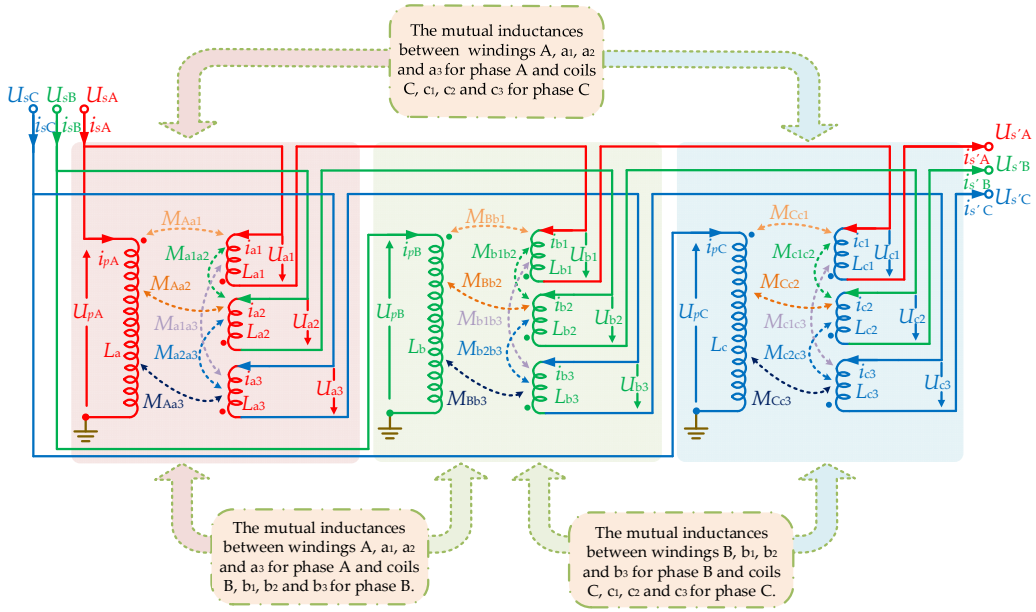

Figure 2. The coupled circuit of the ST.

According to the ST coupled circuit shown in Figure 2, the branch voltage $\boldsymbol{U}_{branch}$ and current $\boldsymbol{i}_{branch}$ for the ST are defined as follows:

$$\boldsymbol{U}_{branch} = \begin{bmatrix} U_{pA} & U_{pB} & U_{pC} & U_{ss'A} & U_{ss'B} & U_{ss'C} \end{bmatrix}^T \quad (1)$$

$$\boldsymbol{i}_{branch} = \begin{bmatrix} i_{pA} & i_{pB} & i_{pC} & i_{s'A} & i_{s'B} & i_{s'C} \end{bmatrix}^T \quad (2)$$

where U_{pA}, U_{pB}, and U_{pC} denote the voltages of the primary windings for the ST, respectively. i_{pA}, i_{pB}, and i_{pC} denote the currents of the primary windings for the ST, respectively. $i_{s'A}$, $i_{s'B}$, and $i_{s'C}$ represent the currents of the secondary windings for the ST, respectively. $U_{ss'A}$, $U_{ss'B}$, and $U_{ss'C}$ represent the voltages of the secondary windings for the ST, and they are given by

$$\begin{cases} U_{ss'A} = U_{a1} + U_{b1} + U_{c1} \\ U_{ss'B} = U_{a2} + U_{b2} + U_{c2} \\ U_{ss'C} = U_{a3} + U_{b3} + U_{c3} \end{cases} \quad (3)$$

The relationship between the branch voltage and branch current can be established as follows:

$$\boldsymbol{U}_{branch} = \boldsymbol{Z}_{branch}\boldsymbol{i}_{branch} \quad (4)$$

where $\boldsymbol{Z}_{branch}$ denotes the branch impedance matrix for ST, and it is described as follows:

$$\boldsymbol{Z}_{branch} = \begin{bmatrix} Z_{sA\_A} & Z_{sA\_B} & Z_{sA\_C} & Z_{sA\_a} & Z_{sA\_b} & Z_{sA\_c} \\ Z_{sB\_A} & Z_{sB\_B} & Z_{sB\_C} & Z_{sB\_a} & Z_{sB\_b} & Z_{sB\_c} \\ Z_{sC\_A} & Z_{sC\_B} & Z_{sC\_C} & Z_{sC\_a} & Z_{sC\_b} & Z_{sC\_c} \\ Z_{s\prime a\_A} & Z_{s\prime a\_B} & Z_{s\prime a\_C} & Z_{s\prime a\_a} & Z_{s\prime a\_b} & Z_{s\prime a\_c} \\ Z_{s\prime b\_A} & Z_{s\prime b\_B} & Z_{s\prime b\_C} & Z_{s\prime b\_a} & Z_{s\prime b\_b} & Z_{s\prime b\_c} \\ Z_{s\prime c\_A} & Z_{s\prime c\_B} & Z_{s\prime c\_C} & Z_{s\prime c\_a} & Z_{s\prime c\_b} & Z_{s\prime c\_c} \end{bmatrix} \quad (5)$$

Indices M, N, m, and n are defined in order to clarify each element in the branch impedance matrix, among M, N = A, B, and C; m, n = a, b, and c, respectively. Equation (5) can then be rewritten as follows:

$$\boldsymbol{Z}_{branch} = \begin{bmatrix} \boldsymbol{Z}_{sM\_N} & \boldsymbol{Z}_{sM\_n} \\ \boldsymbol{Z}_{s\prime m\_N} & \boldsymbol{Z}_{s\prime m\_n} \end{bmatrix} \quad (6)$$

where $\boldsymbol{Z}_{sM\_N}$ represents the mutual inductance between the primary winding in phase M and primary winding in phase N and $\boldsymbol{Z}_{sM\_n}$ denotes the sum of the mutual inductances between the primary winding in phase M and the secondary windings series-connected in the transmission line for phase n. $\boldsymbol{Z}_{s'm\_N}$ denotes the sum of mutual inductances between primary winding in phase N and the secondary windings series-connected in the transmission line for phase m. $\boldsymbol{Z}_{s'm\_n}$ represents the sum of the mutual inductances between the secondary windings series-connected in the transmission line for phase m and the secondary windings series-connected in the transmission line for phase n. Here, $\boldsymbol{Z}_{s\mathrm{A\_A,B,andC}}$, $\boldsymbol{Z}_{s\mathrm{A\_a,b,andc}}$, $\boldsymbol{Z}_{s'\mathrm{a\_A,B,andC}}$, and $\boldsymbol{Z}_{s'\mathrm{a\_a,b,andc}}$ are taken as examples for illustration in Equation (7). The other specific elements in the impedance matrix are shown in Appendix A.

$$\begin{cases} Z_{sA\_A} = Z_{AA} \\ Z_{sA\_B} = Z_{AB} \\ Z_{sA\_C} = Z_{AC} \end{cases} \quad \text{(a)} \qquad \begin{cases} Z_{sA\_a} = Z_{Aa1} + Z_{Ab1} + Z_{Ac1} \\ Z_{sA\_b} = Z_{Aa2} + Z_{Ab2} + Z_{Ac2} \\ Z_{sA\_c} = Z_{Aa3} + Z_{Ab3} + Z_{Ac3} \end{cases} \quad \text{(b)}$$

$$\begin{cases} Z_{s\prime a\_A} = Z_{a1A} + Z_{b1A} + Z_{c1A} \\ Z_{s\prime a\_B} = Z_{a1B} + Z_{b1B} + Z_{c1B} \\ Z_{s\prime a\_C} = Z_{a1C} + Z_{b1C} + Z_{c1C} \end{cases} \quad \text{(c)} \qquad \begin{cases} Z_{s\prime a\_a} = Z_{a1a1} + Z_{a1b1} + Z_{a1c1} + Z_{b1a1} + Z_{b1b1} + Z_{b1c1} \\ \qquad + Z_{c1a1} + Z_{c1b1} + Z_{c1c1} \\ Z_{s\prime a\_b} = Z_{a1a2} + Z_{a1b2} + Z_{a1c2} + Z_{b1a2} + Z_{b1b2} + Z_{b1c2} \\ \qquad + Z_{c1a2} + Z_{c1b2} + Z_{c1c2} \\ Z_{s\prime a\_c} = Z_{a1a3} + Z_{a1b3} + Z_{a1c1} + Z_{b1a3} + Z_{b1b3} + Z_{b1c3} \\ \qquad + Z_{c1a3} + Z_{c1b3} + Z_{c1c3} \end{cases} \quad \text{(d)} \quad (7)$$

Because the expression in Equation (4) cannot fully reflect the mathematical characteristics between the terminals of the ST and the external electrical network, it is necessary to further convert the branch voltage and the branch current into the nodal voltage and the nodal current. Hence, $\boldsymbol{U}_{branch}$ and $\boldsymbol{i}_{branch}$ are replaced by the nodal voltage $\boldsymbol{U}_{node}$ and the nodal current $\boldsymbol{i}_{node}$, and the latter are defined as follows:

$$\boldsymbol{U}_{node} = \begin{bmatrix} U_{sA} & U_{sB} & U_{sC} & U_{s\prime A} & U_{s\prime B} & U_{s\prime C} \end{bmatrix}^T \quad (8)$$

$$\boldsymbol{i}_{node} = \begin{bmatrix} i_{sA} & i_{sB} & i_{sC} & i_{s\prime A} & i_{s\prime B} & i_{s\prime C} \end{bmatrix}^T \quad (9)$$

According to the coupled circuit in Figure 2, $\boldsymbol{U}_{node}$ can be expressed by $\boldsymbol{U}_{branch}$, and the relationship between $\boldsymbol{i}_{branch}$ and $\boldsymbol{i}_{node}$ is also obtained as follows:

$$\begin{aligned} \boldsymbol{U}_{node} &= \boldsymbol{N}_1 \boldsymbol{U}_{branch} \\ \boldsymbol{i}_{node} &= \boldsymbol{N}_2 i_{branch} \end{aligned} \quad (10)$$

where $\boldsymbol{N}_1$ and $\boldsymbol{N}_2$ are the conversion matrices for converting $\boldsymbol{U}_{branch}$ and $\boldsymbol{i}_{branch}$ into $\boldsymbol{U}_{node}$ and $\boldsymbol{i}_{node}$, respectively; they are shown as follows:

$$\boldsymbol{N}_1 = \begin{bmatrix} 1 & 0 & 0 & 0 & 0 & 0 \\ 0 & 1 & 0 & 0 & 0 & 0 \\ 0 & 0 & 1 & 0 & 0 & 0 \\ 1 & 0 & 0 & -1 & 0 & 0 \\ 0 & 1 & 0 & 0 & -1 & 0 \\ 0 & 0 & 1 & 0 & 0 & -1 \end{bmatrix}, \boldsymbol{N}_2 = \begin{bmatrix} 1 & 0 & 0 & 1 & 0 & 0 \\ 0 & 1 & 0 & 0 & 1 & 0 \\ 0 & 0 & 1 & 0 & 0 & 1 \\ 0 & 0 & 0 & 1 & 0 & 0 \\ 0 & 0 & 0 & 0 & 1 & 0 \\ 0 & 0 & 0 & 0 & 0 & 1 \end{bmatrix} \tag{11}$$

By combining Equations (4) and (8)–(11), the relationship between $\boldsymbol{i}_{node}$ and $\boldsymbol{U}_{node}$ can be established:

$$\boldsymbol{i}_{node} = N_2 \boldsymbol{Z}_{branch}^{-1} \boldsymbol{N}_1^{-1} \boldsymbol{U}_{node} \tag{12}$$

The nodal admittance matrix $\boldsymbol{G}_{node}$ for the ST is then defined and expressed as follows:

$$\boldsymbol{G}_{node} = \boldsymbol{N}_2 \boldsymbol{Z}_{branch}^{-1} \boldsymbol{N}_1^{-1} \tag{13}$$

Consequently, a fully decoupled mathematical model for the ST can be constructed according to the nodal admittance matrix $\boldsymbol{G}_{node}$ in Equation (13) and it is shown in Figure 3. The specific elements in Figure 3 are demonstrated in Appendix B.

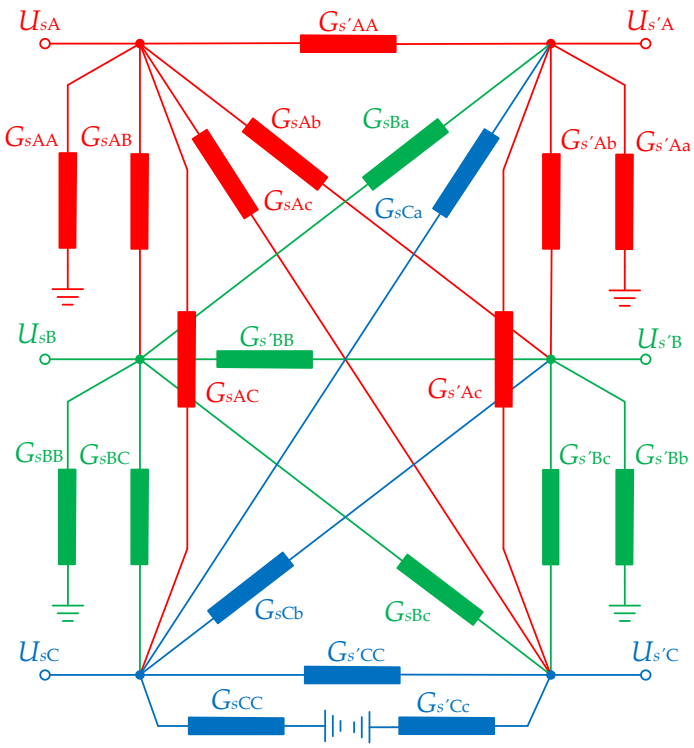

Figure 3. The equivalent decoupled circuit for the ST.

2.3. ST Phase Coordinate Model Incorporating Ground Impedance on Its Primary Side

The established ST model ignores the ground impedance on its primary windings, although this can be an important part of the analysis of a grounding system. Thus, in order to calculate the short-circuit current flowing through the ST in a grounding system precisely, it is necessary to consider the ground impedance of the primary windings for the ST.

The ground impedance is considered to be $\boldsymbol{Z}_{sG}$, and the modified relationship between the branch voltage and branch current can be obtained as follows:

$$\begin{bmatrix} \boldsymbol{U}_{branch} \\ \boldsymbol{U}_{sG} \end{bmatrix} = \underbrace{\begin{bmatrix} \boldsymbol{Z}_{branch} & 0 \\ 0 & \boldsymbol{Z}_{sG} \end{bmatrix}}_{\boldsymbol{Z}'_{branch}} \begin{bmatrix} \boldsymbol{i}_{branch} \\ \boldsymbol{i}_{sG} \end{bmatrix} \tag{14}$$

where $\boldsymbol{Z}_{branch}$ represents the branch impedance matrix for the ST, and $\boldsymbol{U}_{sG}$ and $\boldsymbol{i}_{sG}$ denote the voltage and current of ground impedance, respectively.

Furthermore, the modified branch admittance matrix $\boldsymbol{G'}_{branch}$ is derived as follows:

$$\begin{bmatrix} \boldsymbol{i}_{branch} \\ \boldsymbol{i}_{sG} \end{bmatrix} = \underbrace{\begin{bmatrix} \boldsymbol{Z}^{-1}_{branch} & 0 \\ 0 & \boldsymbol{Z}^{-1}_{sG} \end{bmatrix}}_{\boldsymbol{G'}_{branch}} \begin{bmatrix} \boldsymbol{U}_{branch} \\ \boldsymbol{Z}_{sG} \end{bmatrix} \tag{15}$$

The conversion matrix $\boldsymbol{N}_1$ in Equation (10) may be rewritten as $\boldsymbol{N}_{1'}$:

$$\begin{bmatrix} U_{s\mathrm{A}} \\ U_{s\mathrm{B}} \\ U_{s\mathrm{C}} \\ U_{s'\mathrm{A}} \\ U_{s'\mathrm{B}} \\ U_{s'\mathrm{C}} \\ \ddot{U}_G \end{bmatrix} = \underbrace{\begin{bmatrix} 1 & 0 & 0 & 0 & 0 & 0 & 1 \\ 0 & 1 & 0 & 0 & 0 & 0 & 1 \\ 0 & 0 & 1 & 0 & 0 & 0 & 1 \\ 1 & 0 & 0 & -1 & 0 & 0 & 1 \\ 0 & 1 & 0 & 0 & -1 & 0 & 1 \\ 0 & 0 & 1 & 0 & 0 & -1 & 1 \\ 0 & 0 & 0 & 0 & 0 & 0 & 1 \end{bmatrix}}_{N'_1} \begin{bmatrix} U_{p\mathrm{A}} \\ U_{p\mathrm{B}} \\ U_{p\mathrm{C}} \\ U_{ss'\mathrm{A}} \\ U_{ss'\mathrm{B}} \\ U_{ss'\mathrm{C}} \\ \ddot{U}_{sG} \end{bmatrix} \tag{16}$$

In this way, the conversion matrix $\boldsymbol{N}_2$ in Equation (11) can be modified as $\boldsymbol{N}_{2'}$:

$$\begin{bmatrix} i_{s\mathrm{A}} \\ i_{s\mathrm{B}} \\ i_{s\mathrm{C}} \\ i_{s'\mathrm{A}} \\ i_{s'\mathrm{B}} \\ i_{s'\mathrm{C}} \\ i_G \end{bmatrix} = \underbrace{\begin{bmatrix} 1 & 0 & 0 & 1 & 0 & 0 & 0 \\ 0 & 1 & 0 & 0 & 1 & 0 & 0 \\ 0 & 0 & 1 & 0 & 0 & 1 & 0 \\ 0 & 0 & 0 & 1 & 0 & 0 & 0 \\ 0 & 0 & 0 & 0 & 1 & 0 & 0 \\ 0 & 0 & 0 & 0 & 0 & 1 & 0 \\ 0 & 0 & 0 & 0 & 0 & 0 & 1 \end{bmatrix}}_{N'_2} \begin{bmatrix} i_{p\mathrm{A}} \\ i_{p\mathrm{B}} \\ i_{p\mathrm{C}} \\ i_{s'\mathrm{A}} \\ i_{s'\mathrm{B}} \\ i_{s'\mathrm{C}} \\ i_{sG} \end{bmatrix} \tag{17}$$

Therefore, the modified nodal admittance matrix $\boldsymbol{G}'_{node}$ involving the ground impedance on the ST's primary windings can be acquired as follows:

$$\boldsymbol{G}'_{node} = \boldsymbol{N}'_2 \boldsymbol{G}'_{branch} \boldsymbol{N}'^{-1}_1 \tag{18}$$

3. Short-Circuit Calculation for Electric Power Network Based on the Phase Coordinate Method

3.1. Modeling of Electric Power Network Using the Phase Coordinate Method

An electric power network is usually represented by a nodal admittance network. Therefore, the fault location is added as a new bus to convert the line fault into a bus fault. In this paper, the bus fault is considered in the phase domain.

The nodal network equation of a power system can be described as follows:

$$\begin{bmatrix} \boldsymbol{Y}_{11} & \cdots & \boldsymbol{Y}_{1n} \\ \vdots & & \vdots \\ \boldsymbol{Y}_{n1} & \cdots & \boldsymbol{Y}_{nn} \end{bmatrix} \begin{bmatrix} \boldsymbol{U}_1 \\ \vdots \\ \boldsymbol{U}_n \end{bmatrix} = \begin{bmatrix} \boldsymbol{i}_1 \\ \vdots \\ \boldsymbol{i}_n \end{bmatrix} \tag{19}$$

where $\boldsymbol{Y}_{ij}$ denotes the mutual admittance between the ith bus and the jth bus. $\boldsymbol{i}_i$ denotes current injected at the ith bus, and $\boldsymbol{U}_i$ is the voltage at the ith bus. The specific elements in Equation (19) can be demonstrated as follows:

$$\boldsymbol{Y}_{ij} = \begin{bmatrix} Y_{ij}^{AA} & Y_{ij}^{AB} & Y_{ij}^{AC} \\ Y_{ij}^{BA} & Y_{ij}^{BB} & Y_{ij}^{BC} \\ Y_{ij}^{CA} & Y_{ij}^{CB} & Y_{ij}^{CC} \end{bmatrix}, \boldsymbol{U}_i = \begin{bmatrix} U_{iA} \\ U_{iB} \\ U_{iC} \end{bmatrix}, \boldsymbol{i}_i = \begin{bmatrix} i_{iA} \\ i_{iB} \\ i_{iC} \end{bmatrix}$$

3.2. Single-Phase-to-Ground Fault

When an A-phase-to-ground fault occurs, the voltage at the additional ith bus $U'_{iA} = 0$. Meanwhile, a current source $\boldsymbol{i}_f$ is added as the equivalent short-circuit current at the ith bus, i.e., $\boldsymbol{i}_f = \begin{bmatrix} i_{fA} & 0 & 0 \end{bmatrix}^T$. Equation (19) can then be modified as follows:

$$\begin{bmatrix} \boldsymbol{Y}_{11} & \boldsymbol{Y}_{12} & \cdots & \boldsymbol{Y}_{1i} & \cdots & \boldsymbol{Y}_{1n} \\ \boldsymbol{Y}_{21} & \boldsymbol{Y}_{22} & \cdots & \boldsymbol{Y}_{2i} & \cdots & \boldsymbol{Y}_{2n} \\ \vdots & \vdots & \vdots & \vdots & \vdots & \vdots \\ \boldsymbol{Y}_{i1} & \boldsymbol{Y}_{i2} & \cdots & \boldsymbol{Y}_{ii} & \cdots & \boldsymbol{Y}_{in} \\ \vdots & \vdots & \vdots & \vdots & \vdots & \vdots \\ \boldsymbol{Y}_{n1} & \boldsymbol{Y}_{n2} & \cdots & \boldsymbol{Y}_{ni} & \cdots & \boldsymbol{Y}_{nn} \end{bmatrix} \begin{bmatrix} \boldsymbol{U}_1 \\ \boldsymbol{U}_2 \\ \vdots \\ \boldsymbol{U}_i \\ \vdots \\ \boldsymbol{U}_n \end{bmatrix} = \begin{bmatrix} \boldsymbol{i}_1 \\ \boldsymbol{i}_2 \\ \vdots \\ \boldsymbol{i}_i \\ \vdots \\ \boldsymbol{i}_n \end{bmatrix} + \begin{bmatrix} 0 \\ 0 \\ \vdots \\ \boldsymbol{i}_f \\ \vdots \\ 0 \end{bmatrix} \tag{20}$$

Equation (20) can be further rewritten as

$$\begin{bmatrix} \boldsymbol{Y}_{11} & \boldsymbol{Y}_{12} & \cdots & \boldsymbol{Y}'_{1i} & \cdots & \boldsymbol{Y}_{1n} \\ \boldsymbol{Y}_{21} & \boldsymbol{Y}_{22} & \cdots & \boldsymbol{Y}'_{2i} & \cdots & \boldsymbol{Y}_{2n} \\ \vdots & \vdots & \vdots & \vdots & \vdots & \vdots \\ \boldsymbol{Y}_{i1} & \boldsymbol{Y}_{i2} & \cdots & \boldsymbol{Y}'_{ii} & \cdots & \boldsymbol{Y}_{in} \\ \vdots & \vdots & \vdots & \vdots & \vdots & \vdots \\ \boldsymbol{Y}_{n1} & \boldsymbol{Y}_{n2} & \cdots & \boldsymbol{Y}'_{ni} & \cdots & \boldsymbol{Y}_{nn} \end{bmatrix} \begin{bmatrix} \boldsymbol{U}_1 \\ \boldsymbol{U}_2 \\ \vdots \\ \boldsymbol{U}'_i \\ \vdots \\ \boldsymbol{U}_n \end{bmatrix} = \begin{bmatrix} \boldsymbol{i}_1 \\ \boldsymbol{i}_2 \\ \vdots \\ \boldsymbol{i}_i \\ \vdots \\ \boldsymbol{i}_n \end{bmatrix} \tag{21}$$

where

$$\boldsymbol{U}'_i = \begin{bmatrix} i_{fA} & U'_{iB} & U'_{iC} \end{bmatrix}^T \tag{22}$$

It should be noted that the admittances $\boldsymbol{Y}_{ij}$ and $\boldsymbol{Y}_{ii}$ are modified as follows:

$$\boldsymbol{Y}'_{ij} = \begin{bmatrix} 0 & Y_{ij}^{AB} & Y_{ij}^{AC} \\ 0 & Y_{ij}^{BB} & Y_{ij}^{BC} \\ 0 & Y_{ij}^{CB} & Y_{ij}^{CC} \end{bmatrix}, \boldsymbol{Y}'_{ii} = \begin{bmatrix} -1 & Y_{ii}^{AB} & Y_{ii}^{BC} \\ 0 & Y_{ii}^{BB} & Y_{ii}^{BC} \\ 0 & Y_{ii}^{CB} & Y_{ii}^{CC} \end{bmatrix} \tag{23}$$

In order to apply this calculation method to other short-circuit faults, it is defined that $\boldsymbol{Y}'_{ij} = \boldsymbol{Y}_{ij}\boldsymbol{T}_1$ and $\boldsymbol{Y}'_{ii} = \boldsymbol{Y}_{ii}\boldsymbol{T}_1 + \boldsymbol{T}_2$, and the coefficient matrices $\boldsymbol{T}_1$ and $\boldsymbol{T}_2$ can be deduced:

$$\boldsymbol{T}_1 = \begin{bmatrix} 0 & 0 & 0 \\ 0 & 1 & 0 \\ 0 & 0 & 1 \end{bmatrix}, \boldsymbol{T}_2 = \begin{bmatrix} -1 & 0 & 0 \\ 0 & 0 & 0 \\ 0 & 0 & 0 \end{bmatrix} \tag{24}$$

Meanwhile, the voltage and the short-circuit current at the ith bus can be concluded:

$$\boldsymbol{U}_i = \boldsymbol{T}_1\boldsymbol{U}'_i \tag{25}$$

$$\boldsymbol{i}_f = -\boldsymbol{T}_2\boldsymbol{U}'_i \tag{26}$$

3.3. Other Short-Circuit Faults

For a fault between phase A and B, the voltage at the *i*th bus and the short-circuit current are given as follows:

$$\begin{cases} U_{i\mathrm{A}} = U_{i\mathrm{B}} \\ i_{f\mathrm{A}} = -i_{f\mathrm{B}} \end{cases} \tag{27}$$

$$\boldsymbol{U}_i' = \begin{bmatrix} U_{i\mathrm{A}} & i_{f\mathrm{A}} & U_{i\mathrm{C}} \end{bmatrix}^T \tag{28}$$

In accordance with the calculation method in the previous subsection, the modified admittance matrices $\boldsymbol{Y}_{ii}{}'$ and $\boldsymbol{Y}_{ij}{}'$ can be deduced as follows:

$$\boldsymbol{Y}_{ij}' = \begin{bmatrix} Y_{ij}^{\mathrm{AA}} + Y_{ij}^{\mathrm{AB}} & 0 & Y_{ij}^{\mathrm{AC}} \\ Y_{ij}^{\mathrm{BA}} + Y_{ij}^{\mathrm{BB}} & 0 & Y_{ij}^{\mathrm{BC}} \\ Y_{ij}^{\mathrm{CA}} + Y_{ij}^{\mathrm{CB}} & 0 & Y_{ij}^{\mathrm{CC}} \end{bmatrix}, \boldsymbol{Y}_{ii}' = \begin{bmatrix} Y_{ii}^{\mathrm{AA}} + Y_{ii}^{\mathrm{AB}} & -1 & Y_{ii}^{\mathrm{AC}} \\ Y_{ii}^{\mathrm{BA}} + Y_{ii}^{\mathrm{BB}} & 1 & Y_{ii}^{\mathrm{BC}} \\ Y_{ii}^{\mathrm{CA}} + Y_{ii}^{\mathrm{CB}} & 0 & Y_{ii}^{\mathrm{CC}} \end{bmatrix} \tag{29}$$

The coefficient matrices $\boldsymbol{T}_1$ and $\boldsymbol{T}_2$ are obtained:

$$\boldsymbol{T}_1 = \begin{bmatrix} 1 & 0 & 0 \\ 1 & 0 & 0 \\ 0 & 0 & 1 \end{bmatrix}, \boldsymbol{T}_2 = \begin{bmatrix} 0 & -1 & 0 \\ 0 & 1 & 0 \\ 0 & 0 & 0 \end{bmatrix} \tag{30}$$

Similarly, the coefficient matrices $\boldsymbol{T}_1$ and $\boldsymbol{T}_2$ for different short-circuit faults can be deduced. $\boldsymbol{U}_i{}'$, $\boldsymbol{T}_1$, and $\boldsymbol{T}_2$ for different short-circuit faults are listed in Table 1. Therefore, the admittance matrix can be modified to calculate the short-circuit currents for various short-circuit faults.

Table 1. The coefficient matrices for different short-circuit faults.

Faults	$\boldsymbol{U}_i{}'$	$\boldsymbol{T}_1$	$\boldsymbol{T}_2$
Phase-A-to-ground fault	$\begin{bmatrix} i_{f\mathrm{A}} \\ U_{i\mathrm{B}} \\ U_{i\mathrm{C}} \end{bmatrix}$	$\begin{bmatrix} 0 & 0 & 0 \\ 0 & 1 & 0 \\ 0 & 0 & 1 \end{bmatrix}$	$\begin{bmatrix} -1 & 0 & 0 \\ 0 & 0 & 0 \\ 0 & 0 & 0 \end{bmatrix}$
Phase-A-to-phase-B fault	$\begin{bmatrix} U_{i\mathrm{A}} \\ i_{f\mathrm{A}} \\ U_{i\mathrm{C}} \end{bmatrix}$	$\begin{bmatrix} 1 & 0 & 0 \\ 1 & 0 & 0 \\ 0 & 0 & 1 \end{bmatrix}$	$\begin{bmatrix} 0 & -1 & 0 \\ 0 & 1 & 0 \\ 0 & 0 & 0 \end{bmatrix}$
Both phase-A- and phase-B-to-ground fault	$\begin{bmatrix} i_{f\mathrm{A}} \\ i_{f\mathrm{B}} \\ U_{i\mathrm{C}} \end{bmatrix}$	$\begin{bmatrix} 0 & 0 & 0 \\ 0 & 0 & 0 \\ 0 & 0 & 1 \end{bmatrix}$	$\begin{bmatrix} -1 & 0 & 0 \\ 0 & -1 & 0 \\ 0 & 0 & 0 \end{bmatrix}$
Three-phase fault	$\begin{bmatrix} U_{i\mathrm{A}} \\ i_{f\mathrm{A}} \\ i_{f\mathrm{B}} \end{bmatrix}$	$\begin{bmatrix} 1 & 0 & 0 \\ 1 & 0 & 0 \\ 1 & 0 & 0 \end{bmatrix}$	$\begin{bmatrix} 0 & -1 & 0 \\ 0 & 0 & -1 \\ 0 & 1 & 1 \end{bmatrix}$
Three-phases-to-ground fault	$\begin{bmatrix} i_{f\mathrm{A}} \\ i_{f\mathrm{B}} \\ i_{f\mathrm{C}} \end{bmatrix}$	$\begin{bmatrix} 0 & 0 & 0 \\ 0 & 0 & 0 \\ 0 & 0 & 0 \end{bmatrix}$	$\begin{bmatrix} -1 & 0 & 0 \\ 0 & -1 & 0 \\ 0 & 0 & -1 \end{bmatrix}$
Phase-A-to-ground and phase-B-to-phase C fault	$\begin{bmatrix} i_{f\mathrm{A}} \\ U_{i\mathrm{B}} \\ i_{f\mathrm{B}} \end{bmatrix}$	$\begin{bmatrix} 0 & 0 & 0 \\ 0 & 1 & 0 \\ 0 & 1 & 0 \end{bmatrix}$	$\begin{bmatrix} -1 & 0 & 0 \\ 0 & 0 & -1 \\ 0 & 0 & 1 \end{bmatrix}$

4. Case Studies

4.1. Validation of the Proposed Model

In order to verify the effectiveness of the proposed short-circuit fault model for the ST, case studies were carried out on the equivalent two-bus system shown in Figure 4, involving all possible short-circuit faults. The parameters of the electrical system originate from [14] and are listed in Table 2. The model introduced in [14] is also adopted for comparison in this paper.

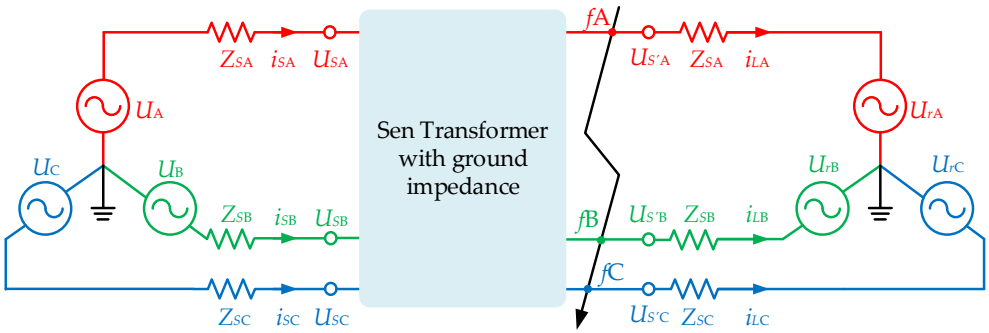

Figure 4. The equivalent circuit diagram for short-circuit analysis.

Table 2. The main parameters and settings for the case studies.

Parameters	Value
Base values	160 MVA, 138 kV
Sending end line-to-line voltage	$1\angle 0^\circ$
Receiving end line-to-line	$1\angle -20^\circ$
Source impedance at the sending end	1.0053 Ω, 19.17 mH
Source impedance at the receiving end	0 Ω, 0 mH
Transmission line impedance	3.0159 Ω, 59.19 mH
Rating of the ST transformer	30 MVA
Single-transformer leakage reactance of the ST	15.73 mH
Ground impedance	4 Ω

Firstly, the number of secondary winding turns for ST was acquired according to the series-connected compensating voltage. The compensating voltage $U_{ss'}$ of 0.2 p.u. at an angle β of 120° was set in this case. Furthermore, the self and mutual inductances of a ST can be calculated based on its unified magnetic equivalent circuit (UMEC), as shown in [17]. Thus, the admittance matrix for the fully decoupled mathematical model of the ST was obtained. Subsequently, the fault voltage vector $\boldsymbol{U}_i'$ and the coefficient matrices $\boldsymbol{T}_1$ and $\boldsymbol{T}_2$ can be obtained based on the types of short-circuit fault, and the admittances $\boldsymbol{Y}_{ii}$ and $\boldsymbol{Y}_{ij}$ in (19) are then modified as $\boldsymbol{Y}_{ii}'$ and $\boldsymbol{Y}_{ij}'$. Consequently, the short-circuit current $\boldsymbol{i}_f$ and voltage $\boldsymbol{U}_f$ for different short-circuit faults can be calculated, as shown in Table 3. Meanwhile, the time-domain simulation results using the PSCAD/EMTDC are also listed in Table 3.

Table 3. The comparison of fault analysis between analytic and simulated studies for different short-circuit faults.

Faults	Simulation Results		Analytic Results		Relative Errors	
	$\begin{bmatrix} U_{s'A} \\ U_{s'B} \\ U_{s'C} \end{bmatrix}$/kV	$\begin{bmatrix} i_{fA} \\ i_{fB} \\ i_{fC} \end{bmatrix}$/kA	$\begin{bmatrix} U_{s'A} \\ U_{s'B} \\ U_{s'C} \end{bmatrix}$/kV	$\begin{bmatrix} i_{fA} \\ i_{fB} \\ i_{fC} \end{bmatrix}$/kA	$\begin{bmatrix} \Delta U_{s'A} \\ \Delta U_{s'B} \\ \Delta U_{s'C} \end{bmatrix}$/%	$\begin{bmatrix} \Delta i_{fA} \\ \Delta i_{fB} \\ \Delta i_{fC} \end{bmatrix}$/%
Phase-A-to-ground fault	$\begin{bmatrix} 0 \\ 77.28 \\ 78.59 \end{bmatrix}$	$\begin{bmatrix} 12.63 \\ 0 \\ 0 \end{bmatrix}$	$\begin{bmatrix} 0 \\ 77.53 \\ 78.17 \end{bmatrix}$	$\begin{bmatrix} 12.58 \\ 0 \\ 0 \end{bmatrix}$	$\begin{bmatrix} 0 \\ 0.32 \\ -0.53 \end{bmatrix}$	$\begin{bmatrix} -0.40 \\ 0 \\ 0 \end{bmatrix}$
Phase-A-to-phase B fault	$\begin{bmatrix} 36.27 \\ 36.27 \\ 72.53 \end{bmatrix}$	$\begin{bmatrix} 12.67 \\ 12.67 \\ 0 \end{bmatrix}$	$\begin{bmatrix} 36.28 \\ 36.28 \\ 72.43 \end{bmatrix}$	$\begin{bmatrix} 12.73 \\ 12.73 \\ 0 \end{bmatrix}$	$\begin{bmatrix} 0.03 \\ 0.03 \\ -0.14 \end{bmatrix}$	$\begin{bmatrix} 0.47 \\ 0.47 \\ 0 \end{bmatrix}$
Both phase-A- and phase-B-to-ground fault	$\begin{bmatrix} 0 \\ 0 \\ 81.24 \end{bmatrix}$	$\begin{bmatrix} 13.95 \\ 13.71 \\ 0 \end{bmatrix}$	$\begin{bmatrix} 0 \\ 0 \\ 81.18 \end{bmatrix}$	$\begin{bmatrix} 13.99 \\ 13.78 \\ 0 \end{bmatrix}$	$\begin{bmatrix} 0 \\ 0 \\ -0.07 \end{bmatrix}$	$\begin{bmatrix} 0.29 \\ 0.51 \\ 0 \end{bmatrix}$
Three-phase-to-ground fault	$\begin{bmatrix} 0 \\ 0 \\ 0 \end{bmatrix}$	$\begin{bmatrix} 14.62 \\ 14.62 \\ 14.62 \end{bmatrix}$	$\begin{bmatrix} 0 \\ 0 \\ 0 \end{bmatrix}$	$\begin{bmatrix} 14.65 \\ 14.57 \\ 14.73 \end{bmatrix}$	$\begin{bmatrix} 0 \\ 0 \\ 0 \end{bmatrix}$	$\begin{bmatrix} 0.21 \\ -0.34 \\ 0.75 \end{bmatrix}$
Phase-A-to-ground and phase-B-to-phase-C fault	$\begin{bmatrix} 0 \\ 46.15 \\ 46.15 \end{bmatrix}$	$\begin{bmatrix} 12.63 \\ 12.66 \\ 12.66 \end{bmatrix}$	$\begin{bmatrix} 0 \\ 45.37 \\ 45.37 \end{bmatrix}$	$\begin{bmatrix} 12.59 \\ 12.61 \\ 12.61 \end{bmatrix}$	$\begin{bmatrix} 0 \\ -1.69 \\ -1.69 \end{bmatrix}$	$\begin{bmatrix} -0.32 \\ -0.39 \\ -0.39 \end{bmatrix}$

It can be seen from Table 3 that the analytic results including the short-circuit current $\boldsymbol{i}_f$ and the voltage $\boldsymbol{U}_f$ at the receiving end of the ST were basically consistent with the simulation results using PSCAD/EMTDC. The range of difference was −1.7–0.027%, which proves the effectiveness of the proposed model. The cause of the difference may be the multi-winding coupling of the ST and the ground impedance on the ST's primary windings, which was ignored in [14]. At the same time, the short-circuit currents were unbalanced for phase A, phase B, and phase C when the symmetrical faults occurred in transmission lines such as the three-phase-to-ground fault. The reason is that the mutual inductances between all windings of the ST were considered in the phase coordinate model for the ST. The mutual inductances between phases were not equal due to the asymmetrical core, resulting in the unbalanced system operation.

4.2. Short-Circuit Current Analysis of ST for Different Operational Modes

Since a ST can inject a variable compensating voltage into the power system, it may have a non-negligible effect on the fault currents flowing through the ST. Therefore, in order to fully analyze the influence of the ST on short-circuit currents in various operational modes, the calculation is carried out under the following conditions: the angle β was varied at a discrete step of 30° in the range of 0° to 360°, and the series-connected compensating voltage of the ST was kept constant at 0.1 p.u. or 0.2 p.u. The variations of short-circuit currents for the single-phase-to-ground and three-phase-to-ground faults at varying phase angles are shown in Figures 5 and 6, respectively.

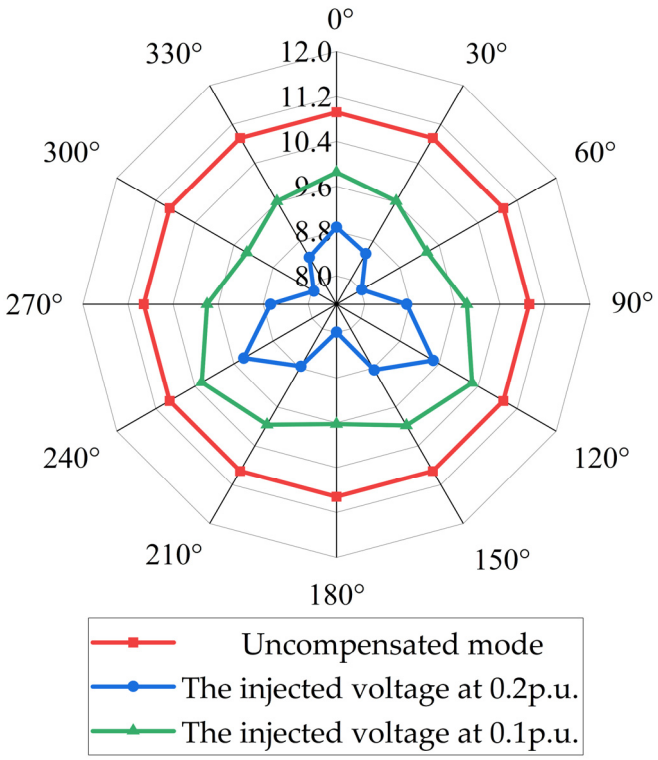

Figure 5. The short-circuit currents for single-phase-to-ground faults.

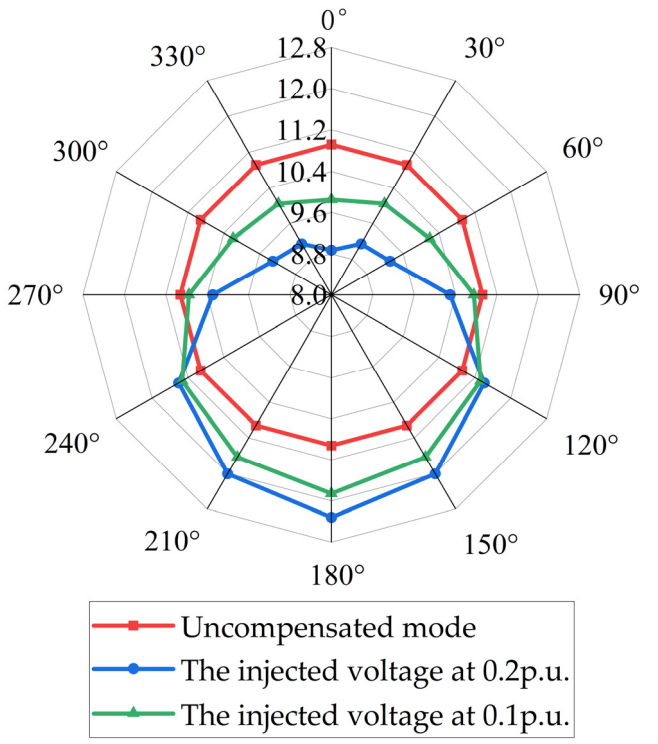

Figure 6. The short-circuit currents for three-phase-to-ground faults.

It can be seen from Figure 5 that the short-circuit current for the compensated mode was less than that for the uncompensated mode during the single-phase-to-ground faults, and the fault current for $U_{ss'}$ = 0.2 p.u. was smallest among them. The trajectories of the short-circuit currents are approximately symmetric about 0°. When the angle of the injected voltage varied from 0° to 180°, the short-circuit current magnitude reached the

maximum at 120° and the minimum at 180°. The variation of the short-circuit currents for the compensated mode can be generalized as a trend of decreasing in the region of 0° to 60° and 120° to 180° and increasing when β was varied from 60° to 120°. The maximum reduction of short-circuit currents reached 27.04% for $U_{ss'}$ = 0.2 p.u. and 14.31% for $U_{ss'}$ = 0.1 p.u. The reasons for the above phenomena in the single-phase-to-ground faults can be described as follows:

1. The dominant components of the series-injected voltage in phase A are the induced voltages from the series windings b1 and c1 when a single-phase-to-ground fault occurs. Because the phase difference between the compensating voltage and the sending-end voltage source in phase A is over 120°, it has a negative effect on the voltage magnitude of phase A and further results in lower fault currents.
2. In the process of increasing β from 0° to 180°, the number of series winding turns showed a trend of increase in the ranges of 0° to 60° and 120° to 180°, and decreased gradually from 60° to 120°. The equivalent impedance brought by the ST followed the same trend as the number of series winding turns. This can explain the opposite phenomenon that happened on the fault currents for the compensated mode.

The short-circuit currents for the three-phase-to-ground faults, as shown in Figure 6, were also symmetric about 0°. However, there were some features different from those shown in Figure 5. In the range of 0° to 180°, the fault currents for the compensated mode were less than those for the uncompensated mode when the angle of injected voltage was less than 90°, and the fault current for $U_{ss'}$ = 0.2 p.u. was less than that for $U_{ss'}$ = 0.1 p.u. The opposite happened when β is greater than 90°. Additionally, both increased gradually in the operational region of 0° to 180°. For the compensating voltage at 0.2 p.u., the short-circuit currents reached a maximum of 12.32 kA and a minimum of 8.87 kA. The short-circuit current reached a maximum of 11.86 kA and a minimum of 9.85 kA when the compensation voltage was equal to 0.1 p.u.

When a three-phase-to-ground fault occurs, a system with a ST can be simplified as shown in Figure 7 by ignoring the asymmetrical mutual inductances between phases in ST. In this situation, the ST can be equivalent to a combination of an ideal ST without internal resistance and an equivalent impedance in series. The fault current flowing through the ST can be approximately calculated as follows:

$$i_{L,ST} = \frac{U}{kZ_S + \frac{Z_{ST}}{k}} = \frac{kU}{|k|^2 Z_S + Z_{ST}} \tag{31}$$

where $k = 1 + \xi e^{j\beta}$, which is the voltage ratio of the ST. ξ stands for the magnitude of the series-connected compensating voltage $U_{ss'}$. Z_{ST} and Z_S represent the equivalent impedances of the ST and the sending end, separately. U denotes the voltage of the sending-end resource.

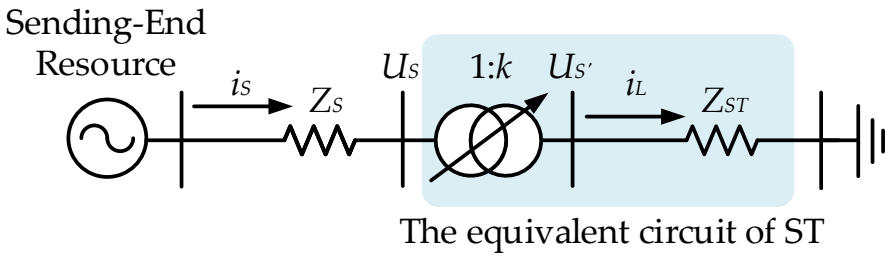

Figure 7. The equivalent circuit after a three-phase-to-ground fault.

It can be seen from Equation (31) that the magnitude of the short-circuit current is mainly affected by $1/|k|$ if Z_{ST} is considered to be 0. The variation of $1/|k|$ with the compensation phase angle is shown in Figure 8.

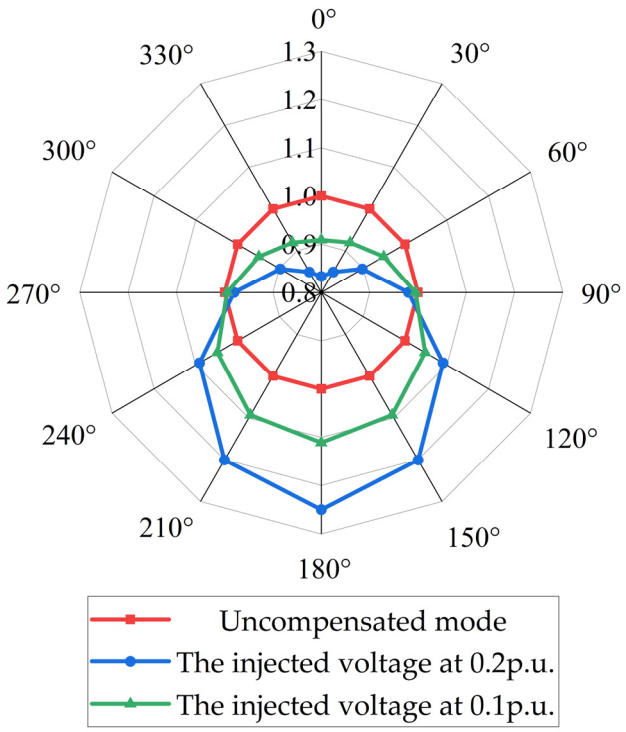

Figure 8. The variation of $1/|k|$ under different phase angles of compensating voltage.

It can be observed from Figure 8 that $1/|k|$ gradually increased in the range of 0° to 180°, which may have caused the same trend of the fault current. Moreover, when the compensation angle was greater than 90°, $1/|k|$ for ξ = 0.1 p.u. was greater than that for ξ = 0.2 p.u. while it was opposite in the range of 0° to 90°. This may lead to the same phenomenon as shown in Figure 6.

From the above cases, the effect of the ST on the fault current is revealed. The effect was variable with the different compensating voltage and fault types. Moreover, it also highlights the potential ability of ST in restraining fault current. In addition, the adjustment of system protection with the addition of a ST is worthy of study.

4.3. Transient Behavior of Different Faults for ST

In order to further study the transient processes of the ST when a short-circuit occurred, the short-circuit model of ST in the phase domain was transformed into the time-domain model. Figure 9 shows the detailed conversion processes of short-circuit model.

In this case, the short-circuit faults were set at the receiving end of the ST and the fault time was set at 0.1 s. The compensating voltage $U_{ss'}$ of 0.2 p.u. was set with the phase angle β of 120°.

In accordance with the proposed method, the short-circuit currents of ST after different faults were obtained as shown in Figure 10.

As shown in Figure 10, the current peak values for the four types of short-circuit fault reached over 20 kA, and decayed to steady-state after 0.18 s. The peak value for the three-phase-to-ground fault was the highest among them, exceeding 25 kA. When a single-phase fault happened, the currents of the other two phases (healthy phases) were also obviously affected. Due to the coupling between the windings of the ST, a fault in any one phase will affect the compensation voltage in other two phases, resulting in the current changes presented in Figure 10a.

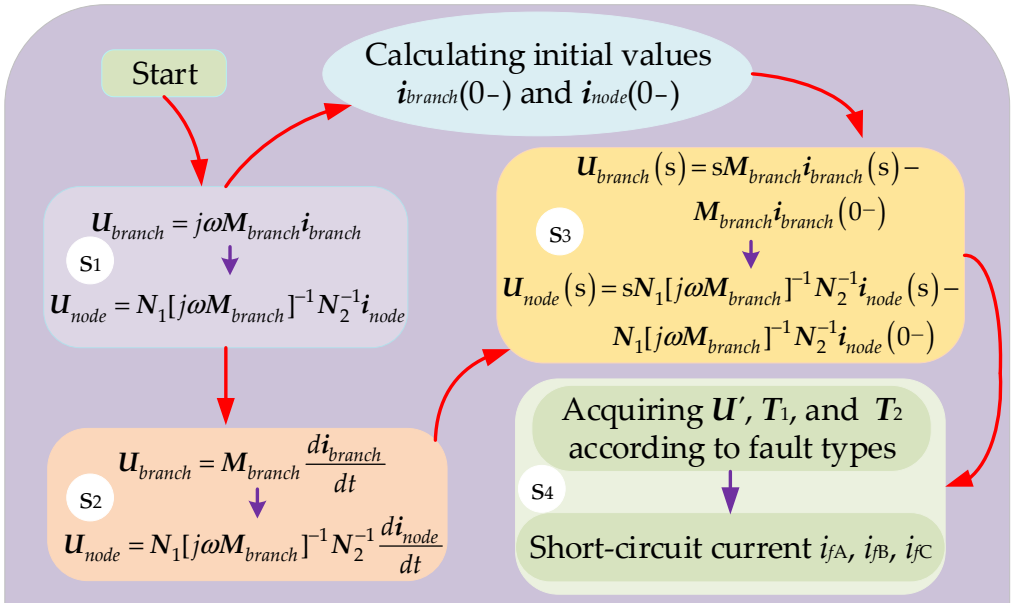

Figure 9. The conversion processes of short-circuit model.

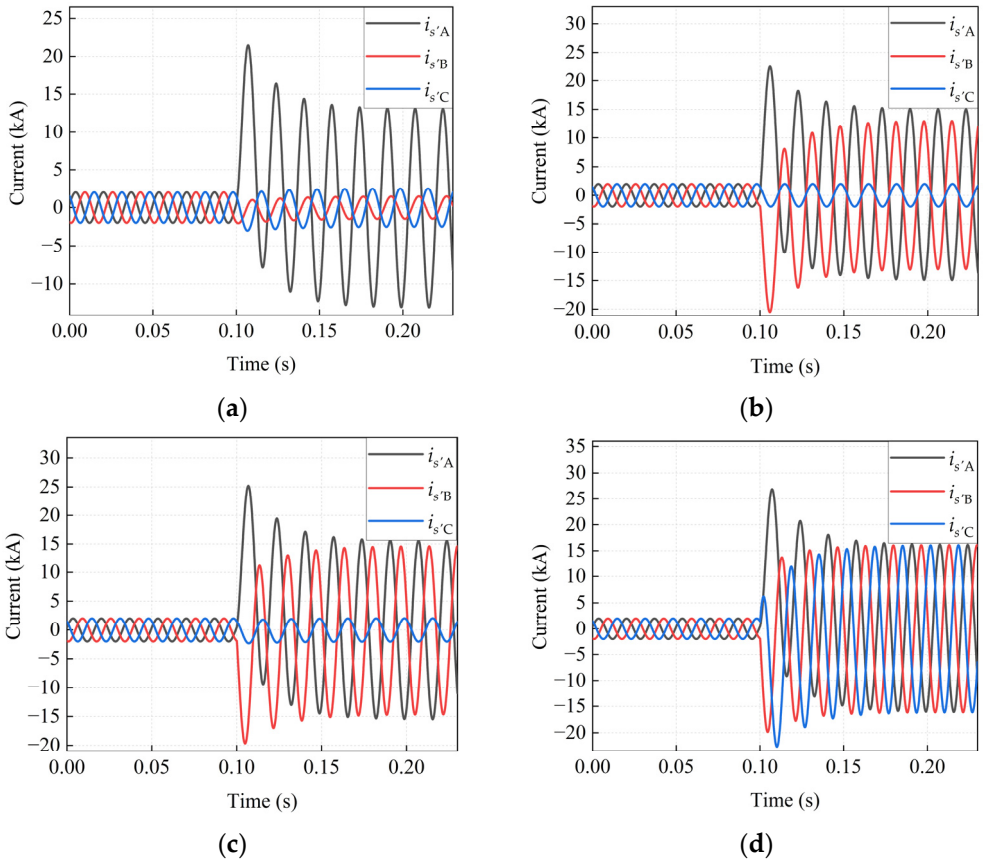

Figure 10. Three-phase fault currents of series windings for (**a**) single-phase-to-ground fault, (**b**) interphase fault, (**c**) two-phase-to-ground fault, and (**d**) three-phase-to-ground fault.

5. Conclusions

In this paper, a short-circuit model of a ST considering the mutual inductance between all windings of the ST and the ground impedance on its primary side for the phase coordinate method is proposed. The validity of the proposed model was verified by

comparison between the results from the analytic calculation utilizing MATLAB and the time-domain simulation using PSCAD/EMTDC. Moreover, additional findings or perceptions were as follows:

1. The results calculated by the proposed method are in good agreement with the simulation results determined using PSCAD/EMTDC, with an error range of −1.69% to 0.75%. Moreover, the proposed phase coordinate model of ST accurately accounted for the mutual inductances between the windings of the ST. The influence of the unbalanced system parameters and ground impedance was also considered in the short-circuit calculation. These factors introduced in the proposed model make it possible to interconnect a ST with the associated grounding system for a proper evaluation of current distribution in the case of ground faults.
2. The effect of the ST on the short-circuit currents was evaluated. It was found that the main influencing factors were the magnitude and phase angle of the compensation voltage and the equivalent impedance, which varied with the number of winding turns. In most cases, it had a negative effect on the short-circuit currents. After a single-phase-to-ground fault occurred, the maximum reduction of short-circuit currents reached 27.04% for the compensating voltage $U_{ss'}$ of 0.2 p.u. and 14.31% when $U_{ss'}$ = 0.1 p.u.
3. The ability of the ST to limit the short-circuit current was identified. This may be a point of concern when designing control strategies for STs. In addition, the impact of this ability on the design and setting of transmission protection systems is worth exploring further.

Author Contributions: Conceptualization, S.H., L.B. and J.F.; methodology, S.H. and L.B.; software, L.B. and J.F.; validation, L.B. and J.F.; formal analysis, L.B.; investigation, L.B. and J.F.; data curation, L.B.; writing—original draft preparation, J.F., L.B. and S.H.; writing—review and editing, S.H., L.B. and J.F.; visualization, L.B. and J.F.; supervision, S.H. All authors have read and agreed to the published version of the manuscript.

Funding: This research was funded in part by the Program for Top Science and Technology Talents in Universities of Guizhou Province under Grant ([2018]036), in part by the Guizhou Province Science and Technology Fund under Grants ([2019]1100/[2021]277).

Institutional Review Board Statement: Not applicable.

Informed Consent Statement: Not applicable.

Data Availability Statement: Not applicable.

Conflicts of Interest: The authors declare no conflict of interest.

Appendix A

The specific elements in the branch impedance matrix (5) are demonstrated as follows:

$$\begin{cases} Z_{s\mathrm{B\_A}} = Z_{\mathrm{BA}} \\ Z_{s\mathrm{B\_B}} = Z_{\mathrm{BB}} \\ Z_{s\mathrm{B\_C}} = Z_{\mathrm{BC}} \end{cases} \quad \begin{cases} Z_{s\mathrm{C\_A}} = Z_{\mathrm{CA}} \\ Z_{s\mathrm{C\_B}} = Z_{\mathrm{CB}} \\ Z_{s\mathrm{C\_C}} = Z_{\mathrm{CC}} \end{cases}$$

$$\begin{cases} Z_{s\mathrm{B\_a}} = Z_{\mathrm{Ba1}} + Z_{\mathrm{Bb1}} + Z_{\mathrm{Bc1}} \\ Z_{s\mathrm{B\_b}} = Z_{\mathrm{Ba2}} + Z_{\mathrm{Bb2}} + Z_{\mathrm{Bc2}} \\ Z_{s\mathrm{B\_c}} = Z_{\mathrm{Ba3}} + Z_{\mathrm{Bb3}} + Z_{\mathrm{Bc3}} \end{cases} \quad \begin{cases} Z_{s\mathrm{C\_a}} = Z_{\mathrm{Ca1}} + Z_{\mathrm{Cb1}} + Z_{\mathrm{Cc1}} \\ Z_{s\mathrm{C\_b}} = Z_{\mathrm{Ca2}} + Z_{\mathrm{Cb2}} + Z_{\mathrm{Cc2}} \\ Z_{s\mathrm{C\_c}} = Z_{\mathrm{Ca3}} + Z_{\mathrm{Cb3}} + Z_{\mathrm{Cc3}} \end{cases}$$

$$\begin{cases} Z_{s\prime\mathrm{b\_A}} = Z_{\mathrm{a2A}} + Z_{\mathrm{b2A}} + Z_{\mathrm{c2A}} \\ Z_{s\prime\mathrm{b\_B}} = Z_{\mathrm{a2B}} + Z_{\mathrm{b2B}} + Z_{\mathrm{c2B}} \\ Z_{s\prime\mathrm{b\_C}} = Z_{\mathrm{a2C}} + Z_{\mathrm{b2C}} + Z_{\mathrm{c2C}} \end{cases} \quad \begin{cases} Z_{s\prime\mathrm{c\_A}} = Z_{\mathrm{a3A}} + Z_{\mathrm{b3A}} + Z_{\mathrm{c3A}} \\ Z_{s\prime\mathrm{c\_B}} = Z_{\mathrm{a3B}} + Z_{\mathrm{b3B}} + Z_{\mathrm{c3B}} \\ Z_{s\prime\mathrm{c\_C}} = Z_{\mathrm{a3C}} + Z_{\mathrm{b3C}} + Z_{\mathrm{c3C}} \end{cases}$$

$$\begin{cases} Z_{s/b\_a} = Z_{a2a1} + Z_{a2b1} + Z_{a2c1} + Z_{b2a1} + Z_{b2b1} + Z_{b2c1} \\ \qquad\qquad + Z_{c2a1} + Z_{c2b1} + Z_{c2c1} \\ Z_{s/b\_b} = Z_{a2a2} + Z_{a2b2} + Z_{a2c2} + Z_{b2a2} + Z_{b2b2} + Z_{b2c2} \\ \qquad\qquad + Z_{c2a2} + Z_{c2b2} + Z_{c2c2} \\ Z_{s/a\_c} = Z_{a2a3} + Z_{a2b3} + Z_{a2c3} + Z_{b2a3} + Z_{b2b3} + Z_{b2c3} \\ \qquad\qquad + Z_{c2a3} + Z_{c2b3} + Z_{c2c3} \end{cases}$$

$$\begin{cases} Z_{s/c\_a} = Z_{a3a1} + Z_{a3b1} + Z_{a3c1} + Z_{b3a1} + Z_{b3b1} + Z_{b3c1} \\ \qquad\qquad + Z_{c3a1} + Z_{c3b1} + Z_{c3c1} \\ Z_{s/c\_b} = Z_{a3a2} + Z_{a3b2} + Z_{a3c2} + Z_{b3a2} + Z_{b3b2} + Z_{b3c2} \\ \qquad\qquad + Z_{c3a2} + Z_{c3b2} + Z_{c3c2} \\ Z_{s/c\_c} = Z_{a3a3} + Z_{a3b3} + Z_{a3c3} + Z_{b3a3} + Z_{b3b3} + Z_{b3c3} \\ \qquad\qquad + Z_{c3a3} + Z_{c3b3} + Z_{c3c3} \end{cases}$$

Appendix B

The specific elements in Figure 3 are demonstrated as follows:

$$\begin{cases} G_{s\mathrm{AA}} = G_{s\mathrm{A\_A}} + G_{s/\mathrm{a\_A}} + G_{s\mathrm{A\_a}} + G_{s/\mathrm{a\_a}} \\ G_{s\mathrm{AB}} = G_{s\mathrm{A\_B}} + G_{s/\mathrm{a\_B}} + G_{s\mathrm{A\_b}} + G_{s/\mathrm{a\_b}} \\ G_{s\mathrm{AC}} = G_{s\mathrm{A\_C}} + G_{s/\mathrm{a\_C}} + G_{s\mathrm{A\_c}} + G_{s/\mathrm{a\_c}} \\ G_{s\mathrm{BB}} = G_{s\mathrm{B\_B}} + G_{s/\mathrm{b\_B}} + G_{s\mathrm{B\_b}} + G_{s/\mathrm{b\_b}} \\ G_{s\mathrm{BC}} = G_{s\mathrm{B\_C}} + G_{s/\mathrm{b\_C}} + G_{s\mathrm{B\_c}} + G_{s/\mathrm{b\_c}} \\ G_{s\mathrm{CC}} = G_{s\mathrm{C\_C}} + G_{s/\mathrm{c\_C}} + G_{s\mathrm{C\_c}} + G_{s/\mathrm{c\_c}} \end{cases} \quad \begin{cases} G_{s/\mathrm{Aa}} = -G_{s/\mathrm{a\_a}} \\ G_{s/\mathrm{Ab}} = -G_{s/\mathrm{a\_b}} \\ G_{s/\mathrm{Ac}} = -G_{s/\mathrm{a\_c}} \\ G_{s/\mathrm{Bb}} = -G_{s/\mathrm{b\_b}} \\ G_{s/\mathrm{Bc}} = -G_{s/\mathrm{b\_c}} \\ G_{s/\mathrm{Cc}} = -G_{s/\mathrm{c\_c}} \end{cases}$$

$$\begin{cases} G_{s/\mathrm{AA}} = -G_{s\mathrm{A\_a}} - G_{s/\mathrm{a\_a}} \\ G_{s\mathrm{Ab}} = -G_{s\mathrm{A\_b}} - G_{s/\mathrm{a\_b}} \\ G_{s\mathrm{Ac}} = -G_{s\mathrm{A\_c}} - G_{s/\mathrm{a\_c}} \\ G_{s\mathrm{Ba}} = -G_{s\mathrm{B\_a}} - G_{s/\mathrm{b\_a}} \\ G_{s/\mathrm{BB}} = -G_{s\mathrm{B\_b}} - G_{s/\mathrm{b\_b}} \\ G_{s\mathrm{Bc}} = -G_{s\mathrm{B\_c}} - G_{s/\mathrm{b\_c}} \\ G_{s\mathrm{Ca}} = -G_{s\mathrm{C\_a}} - G_{s/\mathrm{c\_a}} \\ G_{s\mathrm{Cb}} = -G_{s\mathrm{C\_b}} - G_{s/\mathrm{c\_b}} \\ G_{s\mathrm{Cc}} = -G_{s\mathrm{C\_c}} - G_{s/\mathrm{c\_c}} \end{cases}$$

References

1. Amjad, B.; Al-Ja'afreh, M.A.A.; Mokryani, G. Active Distribution Networks Planning Considering Multi-DG Configurations and Contingency Analysis. *Energies* **2021**, *14*, 4361. [CrossRef]
2. Cui, H.; Li, X.; Wu, G.; Song, Y.; Liu, X.; Luo, D. MPC Based Coordinated Active and Reactive Power Control Strategy of DFIG Wind Farm with Distributed ESSs. *Energies* **2021**, *14*, 3906. [CrossRef]
3. Bifaretti, S.; Bonaiuto, V.; Pipolo, S.; Terlizzi, C.; Zanchetta, P.; Gallinelli, F.; Alessandroni, S. Power Flow Management by Active Nodes: A Case Study in Real Operating Conditions. *Energies* **2021**, *14*, 4519. [CrossRef]
4. Tostado-Veliz, M.; Kamel, S.; Jurado, F. Power Flow Approach Based on the S-Iteration Process. *IEEE Trans. Power Syst.* **2020**, *35*, 4148–4158. [CrossRef]
5. Sen, K.K.; Mey Ling, S. Comparison of the "Sen" transformer with the unified power flow controller. *IEEE Trans. Power Deliv.* **2003**, *18*, 1523–1533. [CrossRef]
6. Sen, K.K.; Mey Ling, S. Introducing the family of "Sen" transformers: A set of power flow controlling transformers. *IEEE Trans. Power Deliv.* **2003**, *18*, 149–157. [CrossRef]
7. Sen, K.K.S. *Introduction to FACTS Controller: Theory, Modeling, and Applications*; IEEE Press and John Wiley: Hoboken, NJ, USA, 2009.
8. Kumar, A.; Sekhar, C. Comparison of Sen Transformer and UPFC for congestion management in hybrid electricity markets. *Int. J. Electr. Power Energy Syst.* **2013**, *47*, 295–304. [CrossRef]
9. Kumar, A.; Gao, W. Power-flow Model of "Sen" Transformer for Loadability Enhancement and Comparison with Unified Power-flow Controllers in Hybrid Electricity Markets. *Electr. Power Compon. Syst.* **2009**, *37*, 189–209. [CrossRef]
10. Gasim Mohamed, S.E.; Jasni, J.; Radzi, M.A.M.; Hizam, H. Implementation of the power transistor-assisted Sen transformer in steady-state load flow analysis. *IET Gener. Transm. Distrib.* **2018**, *12*, 4182–4193. [CrossRef]

11. Gasim Mohamed, S.E.; Jasni, J.; Radzi, M.A.M.; Hizam, H. Power transistor-assisted Sen Transformer: A novel approach to power flow control. *Electr. Power Syst. Res.* **2016**, *133*, 228–240. [CrossRef]
12. Gasim Mohamed, S.E. Power flow control capability of the power transistor-assisted Sen transformer and the unified power flow controller: A close comparison. *IET Gener. Transm. Distrib.* **2020**, *14*, 3033–3041. [CrossRef]
13. Feng, J.; Han, S.; Pan, Y.; Hu, X. Steady-state modelling of Extended Sen Transformer for unified iterative power flow solution. *Electr. Power Syst. Res.* **2020**, *187*, 106492. [CrossRef]
14. Faruque, M.O.; Dinavahi, V. A Tap-Changing Algorithm for the Implementation of "Sen" Transformer. *IEEE Trans. Power Deliv.* **2007**, *22*, 1750–1757. [CrossRef]
15. Asghari, B.; Faruque, M.O.; Dinavahi, V. Detailed Real-Time Transient Model of the "Sen" Transformer. *IEEE Trans. Power Deliv.* **2008**, *23*, 1513–1521. [CrossRef]
16. Liu, J.; Dinavahi, V. Nonlinear Magnetic Equivalent Circuit-Based Real-Time Sen Transformer Electromagnetic Transient Model on FPGA for HIL Emulation. *IEEE Trans. Power Deliv.* **2016**, *31*, 2483–2493. [CrossRef]
17. Pan, Y.; Han, S.; Feng, J.; Hu, X. An analytical electromagnetic model of "Sen" transformer with multi-winding coupling. *Int. J. Electr. Power Energy Syst.* **2020**, *120*, 106033. [CrossRef]
18. Pan, Y.; Han, S.; Zhou, C.; Guo, X. On switching transient modeling and analysis of electronic on-load tap-changers based Sen transformer. *Int. J. Electr. Power Energy Syst.* **2021**, *130*, 107024. [CrossRef]
19. Zhou, C.; Han, S.; Rong, N.; Liu, M. A Duality Based Quasi-Steady-State Model of Three-Phase Five-Limb Sen Transformer. *IEEE Access* **2021**, *9*, 115217–115226. [CrossRef]
20. Abdel-Akher, M.; Nor, K.M. Fault Analysis of Multiphase Distribution Systems Using Symmetrical Components. *IEEE Trans. Power Deliv.* **2010**, *25*, 2931–2939. [CrossRef]
21. Jabr, R.A.; Dzafic, I. A Fortescue Approach for Real-Time Short Circuit Computation in Multiphase Distribution Networks. *IEEE Trans. Power Syst.* **2015**, *30*, 3276–3285. [CrossRef]
22. Ge, Y.; Song, B.; Pei, Y.; Mollet, Y.A.B.; Gyselinck, J.J.C. Analytical Expressions of Isolation Indicators for Permanent-Magnet Synchronous Machines Under Stator Short-Circuit Faults. *IEEE Trans. Energy Convers.* **2019**, *34*, 984–992. [CrossRef]
23. Castro, L.M.; Guillen, D.; Trillaud, F. On Short-Circuit Current Calculations Including Superconducting Fault Current Limiters (ScFCLs). *IEEE Trans. Power Deliv.* **2018**, *33*, 2513–2523. [CrossRef]
24. Dzafic, I.; Jabr, R.A.; Neisius, H.-T. Transformer Modeling for Three-Phase Distribution Network Analysis. *IEEE Trans. Power Syst.* **2015**, *30*, 2604–2611. [CrossRef]
25. Laughton, M.A. Analysis of Unbalanced Polyphase Networks by the Method of Phase Co-ordinates, Part 2. Fault Analysis. *Proc. IEE* **1969**, *116*, 857–865. [CrossRef]
26. Laughton, M.A. Analysis of Unbalanced Poly-phase Networks by the Method of Phase Co-ordinates, Part 1 System Represantation in Phase Frame of Reference. *Proc. IEE* **1969**, *115*, 1163–1172.
27. Gajbhiye, R.K.; Gopi, B.; Kulkarni, P.; Soman, S.A. Computationally Efficient Methodology for Analysis of Faulted Power Systems With Series-Compensated Transmission Lines: A Phase Coordinate Approach. *IEEE Trans. Power Deliv.* **2008**, *23*, 873–880. [CrossRef]
28. Rodriguez, O.; Medina, A. Efficient Methodology for the Transient and Periodic Steady-State Analysis of the Synchronous Machine Using a Phase Coordinates Model. *IEEE Trans. Energy Convers.* **2004**, *19*, 464–466. [CrossRef]
29. Filipović-Grčić, D.; Filipović-Grčić, B.; Capuder, K. Modeling of three-phase autotransformer for short-circuit studies. *Int. J. Electr. Power Energy Syst.* **2014**, *56*, 228–234. [CrossRef]
30. Moorthy, S.S.; Hoadley, D. A new phase-coordinate transformer model for Ybus analysis. *IEEE Trans. Power Syst.* **2002**, *17*, 951–956. [CrossRef]
31. Svenda, G.S.; Nahman, J.M. Transformer phase coordinate models extended for grounding system analysis. *IEEE Trans. Power Deliv.* **2002**, *17*, 1023–1029. [CrossRef]